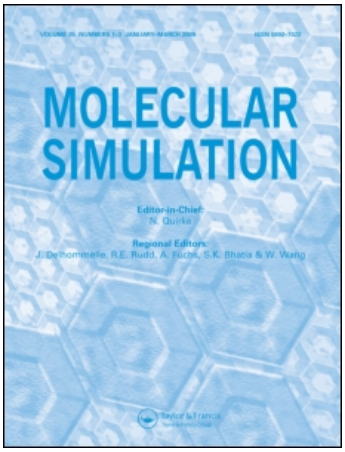

Molecular Simulation
Publication details, including instructions for authors and subscription information:
http://www.informaworld.com/smpp/title~content=t713644482

Formation process, reactivity and physicochemical properties of SiO nanoparticles: spectroscopic and computational study

V. D. Khavryuchenko[a]; O. V. Khavryuchenko[b]; A. I. Brusilovets[b]; V. V. Lisnyak[b]
[a] Institute for Sorption and Problems of Endoecology, National Academy of Sciences of Ukraine, Kyiv, Ukraine [b] Kyiv National Taras Shevchenko University, Kyiv, Ukraine

To cite this Article Khavryuchenko, V. D. , Khavryuchenko, O. V. , Brusilovets, A. I. and Lisnyak, V. V.(2009) 'Formation process, reactivity and physicochemical properties of SiO nanoparticles: spectroscopic and computational study', Molecular Simulation, 35: 5, 358 — 372
To link to this Article: DOI: 10.1080/08927020802616681
URL: http://dx.doi.org/10.1080/08927020802616681

Molecular Simulation
Vol. 35, No. 5, April 2009, 358–372

Taylor & Francis
Taylor & Francis Group

Formation process, reactivity and physicochemical properties of SiO nanoparticles: spectroscopic and computational study

V.D. Khavryuchenko[a1], O.V. Khavryuchenko[b]*, A.I. Brusilovets[b] and V.V. Lisnyak[b2]

[a]*Institute for Sorption and Problems of Endoecology, National Academy of Sciences of Ukraine, Kyiv, Ukraine;* [b]*Kyiv National Taras Shevchenko University, Kyiv, Ukraine*

(*Received 9 October 2008; final version received 11 November 2008*)

Synthesis and spectral (infrared, Raman and inelastic neutron scattering) examination of SiO thin film, powder and products of their oxidation are reported. Processes of SiO formation and interaction with small species, occurring in gas phase, have been simulated in molecular approach by PM3 quantum chemical (QC) method. The QC-simulated model of the SiO nanoparticle was used as a basic model to QC simulate the interaction of SiO molecules and nanoparticle with O_2, CO and H_2O in the cluster approach. Structures of nanoparticles, resulting from such interaction, and their vibrational spectra have been QC simulated. Inverted vibrational problems have been solved in each case in order to verify the QC-evaluated models. Mechanism of the SiO high-temperature oxidation in gas phase is proposed and discussed. QC-evaluated models and complete range of corresponding theoretical and experimental vibration spectra represent molecular interactions with the nanoparticles of SiO and related changes in spectral characteristics.

Keywords: silicon monoxide; silica fume; clusters; amorphous materials; vibrational spectroscopy, quantum chemical simulation; computer simulation

1. Introduction

Silicon monoxide (SiO) is an important material used in thin film optical devices [1–4]. Silicon nanoclusters in the bulk of SiO can emit a light of certain wavelength, governed by the nanoclusters size [4–6]. The technological polymorphism of the SiO formation implies a structural amorphism.

Characterisation and modelling of the amorphous SiO structure are mainly grounded on spectroscopic characteristics, registered for the final product of the gas-phase manufacturing of the SiO-based materials. Nowadays, two basic models of SiO structure are proposed: (1) the model of Si/SiO_2 domains mixture and (2) the model of random bonds. The latter assumes that each Si atom is tetrahedrally coordinated with x O atoms and $4 - x$ Si atoms, and that the $SiSi_xO_{4-x}$ tetrahedron types are distributed statistically [7–17]. It should be also noted that modification of the SiO sample is strictly dependent on the conditions of the deposition, sometimes leading to fibrous colourless samples or reactions of the metal support with the SiO oligomers [18].

None of the aforementioned models can explain the complex structural, chemical and spectroscopic characteristics of the SiO. There are no computational examinations of molecular interactions on the very first stages of the SiO formation and no vibration analysis of SiO_x bulk systems reported in the literature. Moreover, a combined computational and vibrational analysis of the SiO oligomers under matrix-isolation conditions has demonstrated that the mechanisms of oligomerisation and formation of bulk SiO strongly depend on whether the equilibrium state is reached (formation of chain oligomers on the initial stages of the process leads to the fibrous SiO) [18,19]. The spectroscopic analysis, applied for the final products, together with computer modelling can clarify the regularities of both the amorphous SiO structure and its formation process.

Some results of such examination, concerning an atomistic model of the SiO cluster, were presented in [20]. The synthesis, spectral and computational analysis of the SiO thin film, commercial SiO powder produced by CVD method and oxidised SiO film and SiO_2, produced by the SiO powder oxidation, are the issues of the present paper.

The self-synthesised and thermally treated SiO thin films and the commercial SiO and SiO_2 powders have been studied by Fourier-transformed infrared (FTIR), Raman and inelastic neutron scattering (INS) spectroscopy. Also the interaction of SiO clusters with small gaseous molecules (O_2, H_2O and CO) based on the 27SiO model and experimentally measured vibrational spectra is discussed.

Quantum chemical (QC) simulation of the SiO formation and interaction with small gaseous species has been performed. It is known that the formation of the SiO nanoclusters (nanosized supermolecule or particle) occurs in a gas phase upon condensation of the SiO molecules. The thin film of the SiO is formed of those nanoclusters, condensed on the substrate and thus possesses the properties

*Corresponding author. Email: alexk@univ.kiev.ua

ISSN 0892-7022 print/ISSN 1029-0435 online

DOI: 10.1080/08927020802616681
http://www.informaworld.com

of the nanoclusters [21–24]. Therefore, the properties of the SiO gas-phase powder and thin films should by studied based on the cluster (supermolecular) approach.

Formation of the 27SiO cluster, representing the SiO nanoparticle, is QC simulated, followed by simulation of its vibrational spectra and radial distribution function (RDF), which are compared with the experimentally obtained ones. Then interaction of the 27SiO cluster with O_2, CO and H_2O molecules is QC examined based on the cluster approach and using the silica fume (SiO_2) (http://www.ceramite.elkem.com; http://www.silicafume.org/concrete-manual.html) as a reference point of completely oxidised SiO. The silica fume, which is a commercially used material, forms as a result of high-temperature oxidation of SiO nanoparticles during the production of silicon metal or ferroalloys from quartz with coal [25–29].

The experimentally measured IR, Raman and INS spectra of the oxidised SiO film and silica fume (SiO_2) have been compared with the theoretically evaluated spectra of the QC-simulated product of SiO nanoparticle oxidation. The inverted vibrational problem has been solved in respect to three types of experimentally measured vibrational spectra (IR, Raman and INS), in order to assign the bands. The mechanism of the SiO oxidation and the influence of the CO and H_2O molecules on the SiO nanoparticles' properties are discussed in the paper.

2. Experimental

2.1 Materials

2.1.1 Starting materials

A finely dispersed pyrogenic silica (aerosil 380, Degussa) and commercial powder of metallic silicon (Jetmilled Silgrain®, Elkem Materials ASA, Kristiansand, Norway, grain size 150 mkm) have been used for the SiO thin films' synthesis.

2.1.2 Reference materials

The commercial SiO 'Monox Patinal' (Merck, 99% purity), obtained from the pure silicon via a chemical vapour deposition (CVD) process, has been used for the studies as a reference material.

SiO_2 silica fume (microsilica) Grade 940 samples (http://www.ceramite.elkem.com; http://www.silicafume.org/concrete-manual.html; http://www.ceramite.elkem.com/hits/web_0006.nsf/Files/Product-Datasheets-Concrete-Specification/$file/940-Specification-April-2005.pdf) [26,30], produced by Elkem Materials ASA, have been used without any additional treatment. Elkem Microsilica® is produced by the collection and treatment of the fumes released during the manufacturing of ferrosilicon and silicon metal. The process involves reduction of quartz in arc furnaces at temperatures above 2273 K. From the reduction of quartz, SiO gas escapes and mixes with oxygen in the upper part of the furnace, where the SiO oxidises to SiO_2. The latter condenses into spherical particles of the microsilica.

2.2 Synthetic procedures

2.2.1 SiO film synthesis

The synthesis of the SiO thin film is frequently performed by a transport reaction [11], analogously to that reported in [20]. The optical microphotos of the SiO film and commercial powder have been made to study the surface of the samples (refers to Section 3.1).

2.2.2 Thermal treatment

The samples of the synthesised SiO film, commercial SiO powder and the brown by-product, which is probably a fine dispersed mixture of Si and SiO_2, have been loaded into zirconia crucibles and calcined in muffle furnace at air for 4 h at 873 K. The growth in weight of the synthesised SiO film and commercial SiO powder are $\Delta m(SiO_{film}) = 8.9$ mas. %, $\Delta m(SiO_{powder}) = 2.5$ mas. %, respectively. The brown by-product has shown a loss in weight by 18.0 mas. %, probably due to desorption of water, since the product is hygroscopic. A thin layer of white (sometimes brownish) substance showing pronounced chromatism is formed on the surface of the black SiO film upon calcination. The commercial SiO powder does not change colour after thermal treatment.

2.3 Spectroscopic characterisation

2.3.1 FTIR spectroscopy

The IR transmittance and diffusion reflectance Fourier-transformed (FTIR, DRIFT) spectra of the self-synthesised SiO thin film, the commercial SiO sample and the silica fume (SiO_2) were recorded on a Nicolette 320X FTIR spectrometer. The spectral resolution was typically 4 cm^{-1}. The FTIR transmittance spectra have been recorded from the thin layer of pure silica fume samples without dilution, pressed between parallel KBr plates. The attenuated total reflection (ATR) technique was used for the SiO film IR transmittance spectra recording.

2.3.2 Raman spectroscopy

A Jobin Yvon T64000 microspectrometer, operating with argon ion laser (the wavelength of exciting beam is 514.5 nm, the spectral resolution is 1–0.3 cm^{-1}) and equipped with a back-illuminated nitrogen-cooled Spex CCD matrix for signal detection, has been used to record the Raman spectra of the samples. A triple holographic monochromator has been used as a filter. The laser spot diameter, used for the micro-Raman measurements, was

approximately 3–5 μm, and the laser was equipped with 50× ultra long focus Olympus MSPlan objective (numerical aperture = 0.80) for backscattering configuration. The total magnification reached 10, 50 and 100×. Typical recording conditions in the low wave number region are 1800–3600 s.

The optical microphotos of the SiO film, the commercial SiO powder and oxidised SiO film have been photographed by 50× ultra-long-focus Olympus MSPlan objective, mounted on the Raman spectrometer. The reflection mode has been used, since the samples are non-transparent.

2.3.3 INS spectroscopy

The INS spectra of the samples have been measured in the frequency range of 10–10,000 cm^{-1} using the inverted geometry time-of-flight spectrometer and high-resolution NERA-PR spectrometer, installed in the IBR-2 nuclear pulse reactor at the Joint Institute for Nuclear Research, Dubna, Russia (http://www.neutron.anl.gov/mail-archive/0024.html) [31].

All spectra have been recorded at 10 K to reduce the Debye–Waller factor. The pyrolytic graphite analyser with a resolution of *ca.* 2–3% $\Delta E/E$ has been used. The finely ground sample of known weight (approximately 185 g) has been evenly loaded into aluminium foil sachets and mounted onto a centre stick, which had been placed in a closed-cycle refrigerator in the instrument. The sample was then stored for cooling down to 10 K and the INS spectra has been recorded.

2.4 Computational methods and methodology

2.4.1 Methodology

The 'technology-following' methodology [32,33] has been used to simulate the SiO formation and interaction with O_2, H_2O and CO molecules in gas phase. The key idea of this methodology is to reproduce an unknown structure of a product by reproducing the conditions of technological process applied to the known precursors, i.e. the SiO molecules or particles, respectively, in the best possible way. The simulation model is constructed starting from the general data about object structure and experimental properties. The spatial and electronic structures, the force field and the dipole moments derivatives are determined during simulation. These data usually contain two types of errors, namely ones of computational method and the other of model inaccuracies or simplifications. In order to check the value of summary error, one needs to verify model comparing the simulated data with the experimental ones. The verification for crystalline substances is performed using X-ray crystallography by direct comparison of refined structure with the simulated one; sometimes other experimental methods are used depending on the objectives.

Statistical methods of the verification such as vibration spectroscopy [34] and RDF, which express the properties of structural elements assembly, are the main ones in the case of amorphous materials. If there are divergences between the simulated and experimental properties, then the correction of model is performed. Furthermore, the simulation cycle is iterated until the deviation becomes negligible. Such a model is called an adequate to the investigation's objective and is used to determine the physical (the heat of formation, ionisation potential, dipole moment, etc.) and chemical (bonding energy, reactions pathways, etc.) properties. From the point of the formal logic, the 'technology-following' methodology can be classified as a semi-empirical approach, since it combines theoretical speculations with the experimental data.

The 'reaction pathway' methodology [35–38] has been used to simulate the reactions passing through an energy barrier. The distance between two reacting atoms has been frozen and then stepwise decreased by 0.02 nm with complete geometry optimisation of the system, registered at each step, until the reaction energetic barrier is overcome. The QC-evaluated enthalpies of formation of the system, plotted against the distance between two reacting atoms, form a 'reaction profile', making it possible to calculate the energy barrier value (ΔE_i) as a difference between the QC-evaluated enthalpy of formation of the system ($\Delta_f H$) at the transition state and at the conformation, corresponding to the starting energy minimum. The QC-evaluated enthalpy of reaction ($\Delta_r H$) has been calculated as a difference between enthalpies of formation of the system at the starting and final conformations.

2.4.2 QC methods and simulated characteristics

The QC simulation of the SiO nanoparticle formation and its properties has been performed using the semi-empirical PM3 [37,39–42] method in the framework of QuChem software [43], previously approved in the comprehensive investigation of silica and other amorphous materials [34,37,38,44–49]. As a result, the optimised space and electronic structure, force field, dipole moments derivatives and other data have been obtained. The PM3 method is an extension of the modified neglect of diatomic overlap (MNDO) semi-empirical methods line, particularly of the AM1 method. As all semi-empirical methods, the PM3 is set up with the same general structure as a Hartree–Fock calculation in that it has a Hamiltonian and a wave function. The core electrons are not included in the calculation; their effect is considered in the core function – an empirical parametrised formula. The Löwdin-type transformation is applied in order to avoid the time-consuming calculation of three- and four-centre integrals. The PM3 is recommended, since only this method has

some important features for the silica compounds and clusters calculation [49]. Also, as it has been shown in [45], the high bases of *ab initio* methods and PM3 can reproduce the geometry of the siloxanes only. Since the usage of the *ab initio* STO-6G level approximation is hindered by the size of the simulated systems, the choice of the PM3 seems the most preferable.

The COSPECO computation software [50], often applied earlier [45,51–54], has been used to solve the inverted vibrational problem and to verify the simulated data along with the experimental spectra.

The Wiberg index for the bond (W_{AB}) and the sum of Wiberg indices for each atom (W_i), evaluated on the base of the QC computed data, have been used to characterise reactivity of the bonds and atoms. (1) The Wiberg index for the bond (W_{AB}) [55] is determined on the basis of the value of interaction between the atomic orbitals of two atoms. The corresponding equations for the semi-empirical neglected diatomic differential overlap quantum chemistry methods were discussed in [56–59]. (2) An atomic index, i.e. the sum of Wiberg indices for each atom (W_i), is used to determine significant chemical bonds. The W_i is calculated by summing W_{AB} over B neighbours around A. The atomic index W_i is independent on the atom type. It reflects the atomic valence, i.e. a number of electrons participating in the covalent bonds between the *i*-atom and neighbouring ones. From the QC point of view, one can define the W_i value as a coordination number of the *i*-atom.

3. Results and discussion

3.1 Characterisation of the SiO film, powder and products of their oxidation

Optical microphotos of the SiO film, the commercial SiO powder and oxidised SiO film have been photographed in reflection mode in order to characterise their macroscopic structure (Figure 1). As one can see from the Figure 1(a), the upper side of the growing SiO film consists of spherical homogeneous 1–10 mkm particles without microstructure. Particle of the commercial SiO powder has a dendrite structure and consists of the primary particles, smaller than the resolution of the optical microscope. The brownish-black colour of the film indicates a bulky structure of the material, which realizes due to the nature of the support (quartz). It is noteworthy that application of Cu support cooled to 10 K leads to the formation of colourless fibrous samples [4].

The calcining of the SiO film at 873 K at air leads to partial disproportioning of the SiO, resulting in the formation of the metal silicon microparticles (Figure 1(c)). A reflection ability of the film decreases after heating, which affects on the quality of the photos. The macrostructure of the SiO film remains unchanged, except for the microcracks observed. The spherical morphology of the SiO particles is preserved.

Concerning the data on the macrostructure and the weight growth, one can state that neither SiO film nor commercial SiO powder oxidises at 873 K to the SiO_2 completely, but partially disproportionates and forms SiO_x

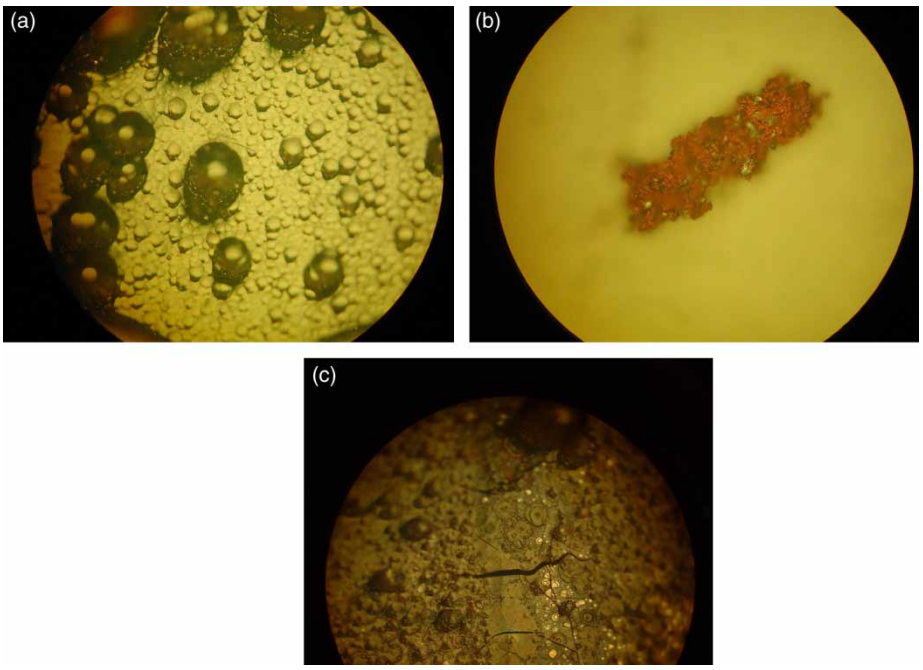

Figure 1. The optical microphotos of (a) the SiO film, magnification 1:100, (b) the commercial SiO powder, magnification 1:100 and (c) oxidised SiO film, magnification 1:200.

($1 < x < 2$) suboxides. Higher temperature is necessary to perform complete oxidation of the SiO. Therefore, the silica fume, which forms upon flame process from the SiO nanoparticles, has been used further as a reference point of a completely oxidised SiO.

3.2 Formation of SiO nanoparticle

3.2.1 Simulation of the SiO nanoparticle formation

The data on the synthesis of the SiO film and characteristics of the SiO commercial powder are given in Section 2. The simulation of the SiO nanoparticle growth in gas phase has been performed in order to analyse the spectral data further.

The spatial structure of the 27SiO cluster was simulated by QC optimisation of randomly oriented 27SiO molecules by energy to the gradient of 0.42 kJ/mol Å. Five different starting geometries have been considered in order to check the adequacy of the model chosen. The simulated $\Delta_f H$ values of the resulting clusters as well as statistical properties, i.e. RDF, bonds length distribution, angles distribution, charge distribution and coordination numbers distribution, can be found in the supplementary materials (Section E). As one can see they are close by values and curves features, one can conclude that the model is adequate and can represent the experimental data on the material.

Cluster 1, representing the condensation of 27SiO molecules, placed in a cubic lattice 3×3 with the edge equal to 1.0835 nm, previously reported at [30], has been chosen as a model of the SiO nanoparticle and further will be referred to as the 27SiO cluster. The Cartesian coordinates of the starting geometry and the space structure of an optimised protoparticle, as well as illustrative movie, can be found in the supplementary materials (Sections A, B1 and D1).

The silicon clusters, identified inside the SiO bulk, varying in size from three to nine Si atoms, are surrounded by the layer of non-stoichiometric SiO_x phase and do not form definitely pronounced domains. The silicon clusters are structurally amorphous, but can crystallise and serve as crystallisation centres at the heating of the SiO particle. Therefore, according to QC simulation results, the model of Si/SiO_2 domains mixture [7–10] and the model of random bonds [7,8,22] do not describe the atomic structure of SiO satisfactorily, because the models operate with the four-coordinated silicon atoms only. The present study demonstrates that Si atoms, especially inside of the silicon clusters, have higher coordination numbers and have a non-tetrahedral coordination surround.

3.2.2 Spectral examination of the SiO

The Raman spectra of the SiO prove the presence of silicon clusters in the SiO bulk of the samples studied

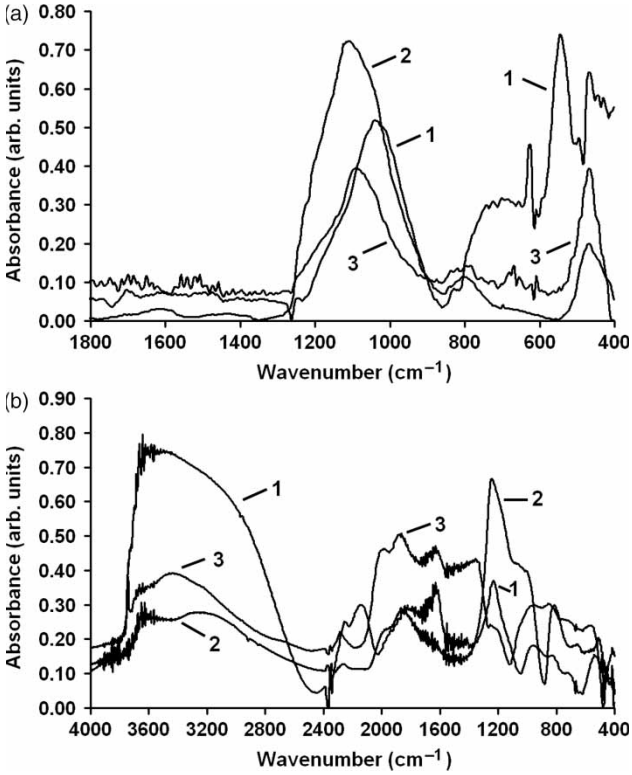

Figure 2. (a) IR transmission and (b) DRIFT spectra of the SiO film (1), commercial SiO powder (2) and oxidised SiO film (3).

(see supplementary materials, Section B2), since highly intensive broad line at 480–500 cm^{-1} can be found. A comparison of FTIR spectra of the SiO with SiO_2 spectra demonstrates that SiO samples cannot be represented as a simple mixture of Si + SiO_2 (Figures 2 and 5).

The inverted vibrational problem has been solved for the QC-simulated IR, Raman and INS spectra, using the experimental spectra of the commercial SiO powder (see supplementary materials, Section B4). The experimental vibration spectra are reproduced by the theoretical model well, therefore the model is adequate to the real SiO particle and can be used for the further QC investigations of the SiO physical and chemical properties.

3.2.3 Analysis of the SiO spectral and QC-simulated data

Analysing the pathway of SiO molecules condensation in 27SiO model (see the movie in supplementary materials, Section A), one can see that $(SiO)_n$ oligomers with Si—Si bonds form at the very first stage of the SiO condensation. The same is observed for models 2–5 (see Section 3.2.1). Also, as it has been previously shown in [20], despite of the fact that the formation of Si—O bonds is energetically preferable, the systems with the Si—Si bonds are observed any time when starting condition is a long distance between two reacting SiO molecules. The formation of the SiO_x layers occurs during the further growth of the

SiO protoparticle. This is strictly contrary to the data of [18,19,60], where cyclic $(SiO)_n$ oligomers with Si—O bonds are unambigously identified as products of the SiO molecules interaction under matrix-isolation conditions.

The discrepancy can be explained by different conditions of the molecular SiO condensation. In the case of [19], reactions are bimolecular and occur at thermodynamic equilibrium, thus the product can relax to more thermodynamically preferable structure, i.e. containing more Si—O bonds. Otherwise, the formation of the SiO protoparticle under flame conditions passes in kinetic mode; consequently Si—Si bonds are conserved, as it is confirmed by Raman spectra [20].

The coordination number distribution for the simulated 27SiO model indicates the non-saturated and non-uniform spatial character of the protoparticle. The simulated RDF reproduces the experimental data of [61] (supplementary materials, Section B6) well. The assignment of the interatomic distances in the simulated RDF (supplementary materials, Section C) shows that the first coordination spheres of atoms in the SiO clusters are narrowly defined, despite the amorphicity of the SiO protoparticle.

Therefore, the structure of the SiO bulk is not quasi-crystalline, but is completely amorphous, i.e. only a close order is observed and the structure is characterised by the distribution of bond lengths, angles and coordination numbers of atoms. The Si atoms' coordination polyhedra often differ from the tetrahedra. This fact affects the chemical properties of the SiO cluster significantly, as it will be demonstrated below.

Humidity and atmosphere contamination affect optical behaviour of SiO greatly, so it is necessary to monitor the interaction of the films with small molecules at least with the main air constituents, such as oxygen, carbon monoxide and water, in order to adapt the SiO-based optical devices.

Since both the gas-phase SiO and SiO thin film consist of nanoparticles, their chemical properties should be simulated in cluster (quasi-molecular) approximation rather than in terms of bulk model. Although the size of the 27SiO particle is small and not enough for the representation of the physical properties of the bulk, e.g. mechanical moduli, the chemical processes can be simulated with sufficient accuracy due to their local character.

3.3 Interaction of SiO with O_2

3.3.1 IR spectral study of the SiO film and commercial powder oxidation products

FTIR analysis of the SiO film oxidised at air at 873 K (Figure 2(a)) shows that the matrix vibrations of the SiO bulk shift after oxidation from 1040, 723 and 626 cm^{-1} to 1092, 796 and 606 cm^{-1}, respectively. As a result, the spectrum of the oxidised SiO film becomes more similar to the spectrum of the SiO commercial powder. The DRIFT spectrum (Figure 2(b)) of the oxidised SiO film in region below 1300 cm^{-1} is almost similar to that of the as-prepared film. However, some differences are observed in the high- and mid-frequency regions, namely the overtones at 1983 and 1882 cm^{-1}, characteristic for the SiO_2 layer, and a narrow intensive band corresponding to the surface Si—OH groups at 3746 cm^{-1} appear in the spectrum of the oxidised SiO film. Bands at 2286 and around 880 cm^{-1}, assigned to the vibrations of the Si—H surface groups [62], remain unchanged. This observation is unexpected, since Si—H surface groups should oxidise to the Si—OH under heating at 873 K.

The DRIFT spectra of the SiO samples exhibit strictly pronounced Christiansen effect [63,64] in the region below 1300 cm^{-1}, i.e. the derivative-like bands are observed instead of the normal Gaussian-shaped ones. It is known that the effect results from the difference in the refraction indices of the transmittance continua and is related to the linear size of the light absorbing body (the linear size of the particle should match the wavelength by an order of magnitude for the effect to occur). The symmetrical vibrational modes are unaffected, while asymmetrical modes produce the derivative-like bands of high intensity to different extend. The spectra with the Christiansen effect still can be analysed in line with the spectra of analogous samples.

The oxidised SiO film exhibits luminescence, so no Raman spectra have been available at the conditions of the spectra sampling.

The IR study of the oxidised SiO film again proves that the heating at 873 K is not sufficient to oxidise the film completely, therefore the product of the higher temperature treatment is necessary as a reference point for the SiO, oxidised to SiO_2 (see Section 3.1).

3.3.2 Interaction of 27SiO cluster with O_2

3.3.2.1 Substantiation and description of starting model. Multiplicity state of molecular or cluster systems at oxidation process is crucial, as it was shown at [65] for Al_n^- clusters. Silicon suboxides, containing metal Si clusters in the bulk, can be treated in the same way, hence different multiplicity states of the $(SiO)_n$ should be concerned.

The main causes are as follows: (1) the O_2 molecules are in the triplet (^3T) ground state, (2) similarly, the SiO nanoparticle might transfer into high-multiplicity state from ^1S due to the presence of Si cluster and Si/SiO_x interface, while the final product is obviously singlet (^1S). The oxidation reaction is multistage and the moment of $^3T \rightarrow {}^1S$ transition is unknown.

The dependence of the enthalpy of formation of the 27SiO cluster on the multiplicity state has been QC examined. Figure 3 shows that the ^3T state is the most energetically stable for the cluster, while other high-multiplicity states, which reach 13, are more stable than

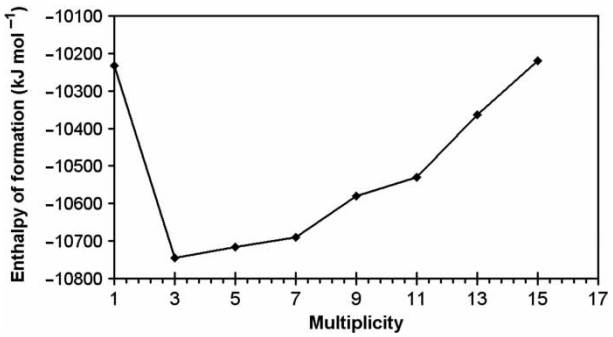

Figure 3. Dependence of the enthalpy of formation of the 27SiO cluster on the multiplicity state.

Table 1. The QC-calculated enthalpies of formation ($\Delta_f H$) of the ($27SiO + O_2$) system at different multiplicity states.

Multiplicity	$\Delta_f H$ (kJ mol^{-1})
1	− 10,240.89
3	− 10,250.97
5	− 10,200.76

the ^1S state. So, interplays between the electronic states of the SiO nanoparticle and O_2 molecule may occur.

At that, the results of the QC calculations, shown at the Table 1, indicated that ^3T is the ground state of ($27SiO + O_2$) system completely optimised by energy. The unpaired electrons are localised at the oxygen molecule; thus, the SiO nanoparticle is in the ^1S state.

Therefore, two following possible mechanisms (further – mechanism (I) and mechanism (II)) have been QC examined, respectively:

$$\begin{aligned} &SiO_x + O_2 \xrightarrow{\Delta E_1, -\Delta_r H_1} \underset{^3T}{SiO_x[O_2]} \xrightarrow{\Delta E_2, -\Delta_r H_2} \underset{^3T}{(SiO_x)O^{\bullet -}} \\ &\quad + O^{\bullet -} \xrightarrow{\Delta E_3, -\Delta_r H_3} \xrightarrow{\Delta E_3, -\Delta_r H_3} \underset{^3T}{(SiO_x)} \\ &\quad - OO \xrightarrow{\Delta_r H_4} \underset{^1S}{(SiO_x)} - OO \end{aligned} \qquad \text{(I)}$$

$$\begin{aligned} &\underset{^3T}{SiO_x} + O_2 \xrightarrow{\Delta E_1, -\Delta_r H_1} \underset{^3T}{SiO_x[O_2]} \xrightarrow{-\Delta_r H_2} \underset{^1S}{(SiO_x)} \\ &\quad - O_2 \xrightarrow{\Delta E_3, -\Delta_r H_3} \xrightarrow{\Delta E_3, -\Delta_r H_3} \underset{^1S}{(SiO_x)} - OO \end{aligned} \qquad \text{(II)}$$

The results show that the activation barriers for the mechanism (II) are much higher than that for the mechanism (I). This is explained by the formation of relatively stable peroxide group at ^1S state of $(SiO_x)O_2$ transition complex. Therefore, the mechanism (I) will be discussed further only.

The following methodology has been used for the QC simulation of the SiO nanocluster oxidation. The most unsaturated surface silicon atom had been chosen as an active centre, i.e. the reacting silicon atom should have the lowest sum of Wiberg indices (refer to the section 2.4.2.). The distance between the closest oxygen atom and the selected silicon atom has been frozen and the 'reaction pathway' methodology has been applied (see Section 2.4.1), resulting in the product of the O_2 molecule chemisorption on the SiO nanoparticle surface. The most reactive of the neighbouring silicon atoms has been chosen after the chemisorption, and the distance between that silicon atom and the second oxygen atom of the O_2 molecule has been frozen and then the 'reaction pathway' methodology has been applied to the atomic pair. Finally, the electronic state of the system has been changed from ^3T to ^1S, and the resulting cluster has been QC optimised by energy. The energetic and magnetic characteristics of the QC-simulated systems are listed in Table 2.

Since the structure of the SiO is amorphous, a set of reactive centres is present on the surface of the SiO particle. Therefore, the simulated reaction pathways and the corresponding enthalpies are not unique but represent the most energetically probable trajectories and thermodynamic characteristics of the reaction.

3.3.2.2 Detailed description of the SiO cluster oxidation. According to the mechanism (I), oxidation includes the following four key stages: (1) chemisorption of the O_2 molecule, (2) dissociation of the O_2 molecule, (3) bonding of the second O atom to the silicon and (4) electronic $^3T \rightarrow {}^1S$ transition. Each of the stages is characterised by the energy barrier (ΔE_i) and the enthalpy of the reaction ($\Delta_r H_i$), listed in Table 3. The energy barrier of the third stage ΔE_3 is negligibly low (less than 5 kJ/mol). The third stage often passes without energy barrier, merging with the second stage.

The oxidation stages can be illustrated by the reaction of the 27SiO cluster with the first O_2 molecule:

$$Si_{27}O_{27} + O_2 = Si_{27}O_{29}.$$

The chemisorption as the first stage of mechanism (I) (Figure 4(b)) results in formation of the O_2 complex:

$$Si_{27}O_{27} + O_2 = Si_{27}O_{27}[O_2].$$

The second stage, i.e. the dissociation of the O_2 molecule (Figure 4(c)), results in the formation of cation radical, located on the nanoparticle bulk, and the 'free' anion-radical $O^{\cdot -}$:

$$Si_{27}O_{27}[O_2] = Si_{27}O_{28}^{+} + O^{\cdot -}.$$

The third stage, i.e. the attachment of the second O atom to the silicon (Figure 4(d)), results in the recombination of the radicals and formation of the neutral

Table 2. The QC-derived characteristics of the simulated clusters: the enthalpy of system formation ($\Delta_f H$), the first ionisation potential (I) and the dipole moment (D).

System	$\Delta_f H$ (kJ mol^{-1})	I (eV)	D (Debye)	Comments
27SiO_O2	− 10,240.89	6.06006	14.19473	Refers to Figure 4(a)
	− 10,250.97	6.05612	14.24463	Refers to Figure 4(b)
	− 10,162.45	5.87684	9.82066	Refers to Figure 4(c)
	− 10,984.07	5.50728	14.99995	Refers to Figure 4(d)
	− 11,094.45	6.25503	13.65855	Refers to Figure 4(e)
27SiOW	− 10,782.91	5.86644	19.60359	Refers to Figure 6(c)
27SiO2W	− 11,079.10	5.73275	20.14149	Refers to Figure 6(d)
	− 11,332.28	5.19611	23.3314	Refers to Figure 6(e)
27SiO2_W	− 23,145.12	5.98263	29.24876	Refers to Figure 7(a)
	− 23,200.88	6.02038	30.45736	Refers to Figure 7(b)
	− 23,107.50	5.20326	34.59838	Refers to Figure 7(c)
	− 23,301.08	5.96587	27.49045	Refers to Figure 7(d)
	− 23,219.87	5.84451	23.52289	Refers to Figure 7(e)
	− 23,329.77	5.82187	21.29860	Refers to Figure 7(f)
27SiO2_2W	− 23,454.01	5.77848	20.65017	Refers to Figure 7(g)

silicon suboxide nanoparticle:

$$Si_{27}O_{28}^{+} + O^{\cdot -} = Si_{27}O_{29}.$$

The fourth stage, i.e. the $^3T \rightarrow {}^1S$ transition (Figure 4(e)), leads to the change of the nanoparticle spatial structure. As one can see, the reaction of the 27SiO cluster with O_2 molecule shares some features with Al_n^- clusters oxidation [65], when concerning the mechanism and stages.

The reactions with other O_2 molecules occur analogously, although the second and third stages sometimes merge. The second oxygen molecule addition is also specific, since the first stage of the reaction (chemisorption) occurs without energy barrier. About 13.5 O_2 molecules are required to be attached to the 27SiO nanoparticle to oxidise the cluster to SiO_2. The step-by-step addition of O_2 molecules continued up to the saturated particle (13 molecules attach); the 14th O_2 molecule's reaction with the nanoparticle has been simulated for the first O atom of O_2 only, while the second O atom is simply removed from the system.

The enthalpies of formation of the products of each oxidation reaction ($\Delta_f H$) in the ^3T and ^1S states, the enthalpies of each reaction ($\Delta_r H$), the enthalpies ($\Delta_r H_1$, $\Delta_r H_2$) and the energy barriers (ΔE_1, ΔE_2) of the first and second stages are presented in the Table 3. The overall enthalpy of the 27SiO nanoparticle oxidation to $27SiO_2$ is equal to − 12449.77 kJ/mol or − 461.12 kJ/mol per one SiO unit: in other words, the reaction is extremely exothermic. The overall enthalpy of the reaction is sufficient to melt the resulting SiO_2 particle.

The mechanism of SiO oxidation is a relay-race process, when an elementary act of oxidation involves all the nanoparticle of SiO due to energetic and structural factors.

Table 3. The enthalpies of formation of the products of the oxidation reaction ($\Delta_f H$) in ^3T and ^1S states, the enthalpies of each reaction ($\Delta_r H$), the enthalpies of electronic $^3T \rightarrow {}^1S$ transitions, the enthalpies ($\Delta_r H_1$, $\Delta_r H_2$) and the energy barriers (ΔE_1, ΔE_2) of the first and second stages (in kJ mol^{-1}).

No.of O_2 mol.	ΔE_1	ΔE_2	$\Delta_r H_1$	$\Delta_r H_2$	Overall $\Delta_r H$ (^3T)	$\Delta_f H$ (^3T)	$\Delta_f H$ (^1S)	Enthalpy of electronic $^3T \rightarrow {}^1S$ transition
1	0	90.89	− 10.08	− 733.07	− 743.19	− 10,984.05	− 11,094.47	− 110.38
2	0	706.81	–	− 571.41	− 571.41	− 12,234.94	− 12,227.75	7.18
3	6.13	37.8	− 124.66	− 497.95	− 622.61	− 12,977.20	− 12,956.79	20.41
4	3.07	43.01	− 209.29	− 891.53	− 1100.82	− 14,217.97	− 14,198.02	19.95
5	14.57	23.35	− 31.54	− 638.53	− 670.07	− 14,866.15	− 15,384.18	− 518.03
6	2.23	13.73	− 183.96	− 548.31	− 732.31	− 15,592.25	− 15,478.43	113.82
7	1.18	35.57	− 217.39	− 907.87	− 1125.26	− 16,701.43	− 16,810.50	− 109.07
8	1.60	116.26	− 116.68	− 594.17	− 710.85	− 17,537.31	− 17,524.21	13.10
9	13.06	31.92	− 31.42	− 493.88	− 525.25	− 18,065.75	− 18,935.70	− 869.95
10	6.47	37.67	− 171.28	− 479.68	− 650.92	− 19,598.00	− 19,723.03	− 125.03
11	10.00	30.03	− 78.75	− 517.15	− 595.90	− 20,332.75	− 20,387.30	− 54.60
12	2.86	51.62	− 142.17	− 768.52	− 910.69	− 21,312.61	− 21,408.07	− 95.47
13	2.77	16.42	− 329.49	− 379.93	− 709.42	− 22,005.23	− 22,312.88	− 307.61
14	3.86				− 363.51	− 22,690.29	− 22,799.91	− 109.62

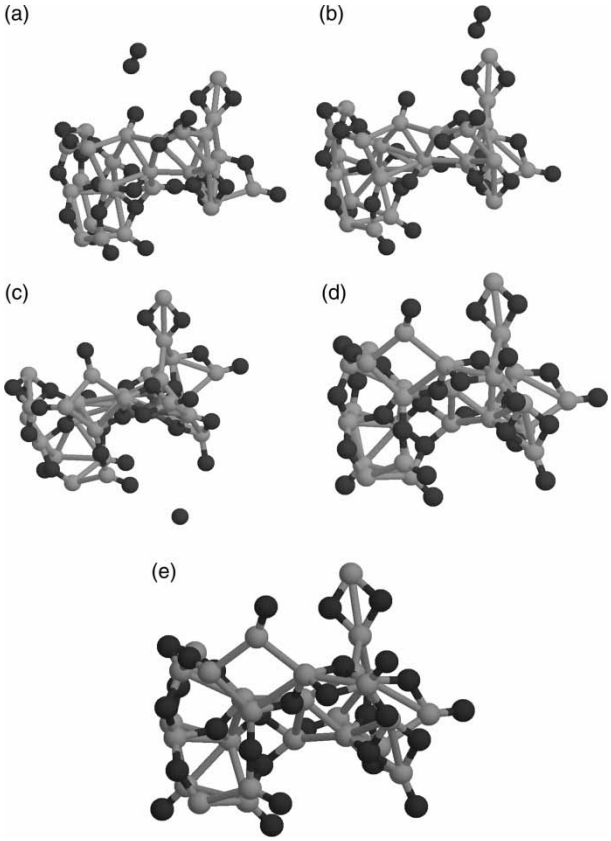

Figure 4. The 27SiO_O2 system, denoting the QC-optimised configurations along the reaction of the 27SiO cluster with the O_2 molecule: (a) starting configuration, (b) chemisorbed O_2 molecule, (c) dissociation of the O_2 molecule, (d) attachment of the second O atom and (e) the QC optimised configuration after the $^3T \rightarrow {}^1S$ transition.

(1) The energetic factor results in great amount of heat educed during each oxidation reaction. The energy of the reaction partially transfers to the vibrational levels of excitation of the particle, sometimes leading to the changes in atoms' connectivity.
(2) The effect of the structural factor is governed by the amorphicity of the SiO nanoparticle and non-tetrahedral coordination of Si atoms. The coordination number of the surface Si atoms grows from three to four upon oxidation, leading to drastic changes in Si coordination polyhedra from quasi-triangle or slightly pyramid to quasi-tetrahedron. These changes provoke relay-race change in the structure of the neighbouring silicon atom polyhedron. Due to the amorphicity of the SiO, space inside the particle is sufficient for rotation of Si-based polyhedra around interatomic bonds and for transfer of O atoms from one silicon polyhedron to another. Thus, the silicon clusters, which are found inside the SiO bulk, are oxidised and then are drawn into the SiO_x phase. The oxidation process also leads to the densifying of the nanoparticle, as the volume of the resulting SiO_2 nanoparticle is lower by 12.5% in comparison with the nanoparticle of the same composition, representing fumed silica [48]. Therefore, the nanoparticle, formed upon the oxidation of the 27SiO nanoparticle, will further be denoted as 'densified silica'. The $\Delta_f H$ of the densified silica nanoparticle is 188.37 kJ/mol less than that of the fumed silica nanoparticle, indicating its lower chemical activity.

It is noteworthy that the starting molecular precursor is obviously of great importance for the structure of the resulting SiO_2 particle. As it just has been pointed above, the molecular SiO condensation under non-equilibrium conditions should lead to bulky $(SiO)_n$ protoparticles with Si—Si bonds, which result in dense quasi-spherical SiO_2 protoparticles under oxidation. Oppositely, the condensation of linear chain $(SiO_2)_n$ oligomers, which are obtained by oxidation of $(SiO)_2$, may result in fibrous SiO_2 [18].

3.3.2.3 Vibrational spectroscopic analysis of the SiO_2 silica fume: Experimental and simulated data. The $27SiO_2$ model of the densified silica has been used for the QC simulation of the IR, Raman and INS spectra. The inverted vibrational problem has been solved for the QC-simulated IR, Raman and INS spectra, using the experimental spectra of the silica fume (SiO_2). The Figure 5 shows that the theoretical model reproduces the experimental vibration spectra well: therefore, the model is adequate to the real densified silica fume particle. The spectra are typical for amorphous silica [48], although the ν^{as}_{Si-O} bands between 1050 and 1250 cm^{-1} in the INS spectrum are strictly resolved, and the significant presence of Si—Si bonds is observed according to the peaks at 480–520 cm^{-1} of the Raman spectrum. So, the QC-simulated oxidation of the SiO nanoparticle with the O_2 has been experimentally proved.

Since the silica fume particles have some adsorbed water on their surfaces, affecting the spectral properties in the high-frequency region of vibrational spectra significantly, the comparison of the QC-evaluated vibrational spectra with the experimental ones will be carried out in Section 3.4.3, after the description of interaction of the resulting $27SiO_2$ nanoparticle with the water.

3.4 Interaction of SiO with H_2O

3.4.1 Influence of the H_2O molecules on the growth of the SiO particle

Interaction of SiO molecules with H_2O in different proportions has been QC examined in order to study the influence of water on the SiO protoparticle formation. The following $SiO:H_2O$ ratios, denoted as clusters 24SiO3W, 18SiO9W, 14SiO13W, 9SiO18W and

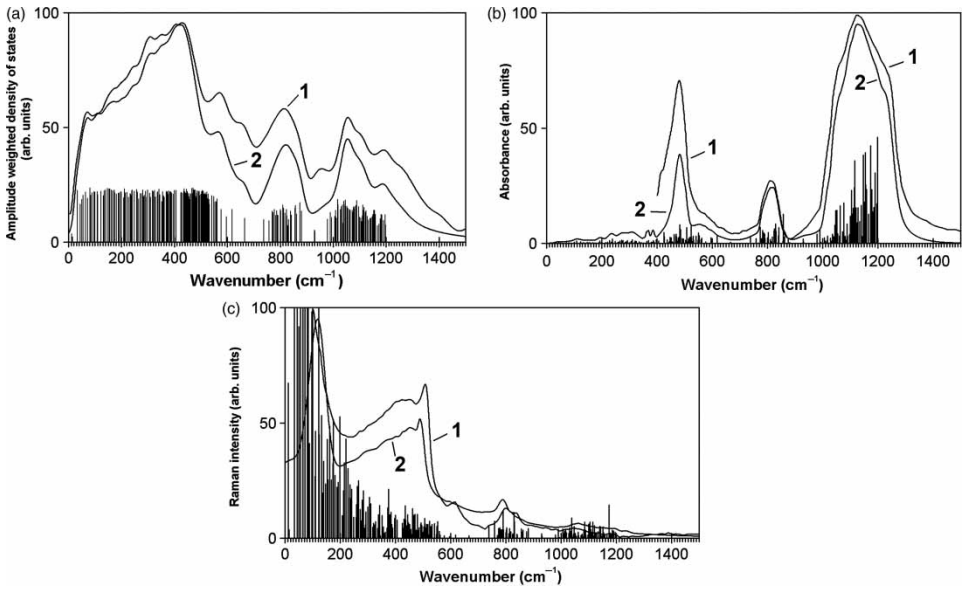

Figure 5. The QC-simulated vibrational spectra of the $27SiO_2$ model of the densified silica, fitted along the experimental spectra of the silica fume: (a) INS, (b) FTIR and (c) Raman spectra. Line (1) – experimental spectrum, line (2) – simulated spectrum. Delta functions of the QC-simulated vibrational modes are represented as thin solid sticks in all figures.

3SiO24W, correspondingly, have been considered: 24:3, 18:9, 14:13, 9:18 and 3:24.

The starting configurations of the systems have been obtained by replacing the corresponding quantity of SiO molecules in the starting configuration of the 27SiO system (see Section 3.2.1). The geometry of the systems has been QC optimised by energy. The QC-evaluated data show that water molecules can form strong H-bonds with the onefold-coordinated O atoms of the SiO cluster and coordinate via oxygen atoms to the unsaturated silicon atoms of the SiO cluster surface. However, the presence of water prevents both the condensation of SiO molecules to the nanoparticle and the formation of Si clusters inside the SiO nanoparticle bulk.

3.4.2 Interaction of 27SiO nanoparticle with H_2O

The interaction of the SiO nanoparticle with water has been QC studied using two models, particularly, 27SiOW and 27SiO2W, referring to the systems of 27SiO nanoparticle with 1 and 2 water molecules, respectively. In both cases, the isolated water molecules react with the SiO nanoparticle similarly: for this reason, the results will be discussed at the same section.

The water molecule absorbs on the SiO nanoparticle surface without activation barrier. Oxygen atom forms a strong coordination bond Si—O ($W_{Si—O} = 0.5508$), while the hydrogen additionally stabilises the sorption complex via H-bonding to the neighbouring onefold-coordinated surface oxygen atom ($W_{O—H} = 0.1025$) (Figure 6). After that, the disproportionation of water may occur ($\Delta E = 25.14$ kJ/mol, $\Delta_r H = -66.52$ kJ/mol), resulting in two surface hydroxyl groups. The QC simulation shows that the formation of the Si—H bond through the disproportionation of water is impossible, and the resulting structure is unstable and relaxes back to the starting configuration.

Therefore, the interaction of the SiO nanoparticle with water may lead to the formation of strongly coordinationally bonded water on the surface of the cluster or to the hydroxylation of the surface.

3.4.3 Interaction of $27SiO_2$ nanoparticle with H_2O

An adequate model is required in order to simulate the vibrational spectra of the densified silica nanoparticle and, thus, to verify the correctness of the QC simulation of the SiO nanoparticle interaction with the O_2 molecules. Since the silica fume, used as a reference point for the verification, absorb water, the QC study of the densified silica nanoparticle with water has been performed before the simulation of vibrational spectra.

Reaction of the $27SiO_2$ nanoparticle with the water molecule is multistage (Figure 7). First, the H_2O molecule absorbs on the densified silica surface without activation barrier (enthalpy of reaction $\Delta_r H = -55.78$ kJ/mol). Second, the proton transfer occurs from the oxygen of water molecule to the onefold-coordinated oxygen of the densified silica nanoparticle, resulting in surface Si—OH group with strongly bonded OH residue ($\Delta E = 93.37$ kJ/mol, $\Delta_r H = 93.37$ kJ/mol).[3] Then the OH residue bonds to the same silicon atom, forming silandiolic $Si(OH)_2$

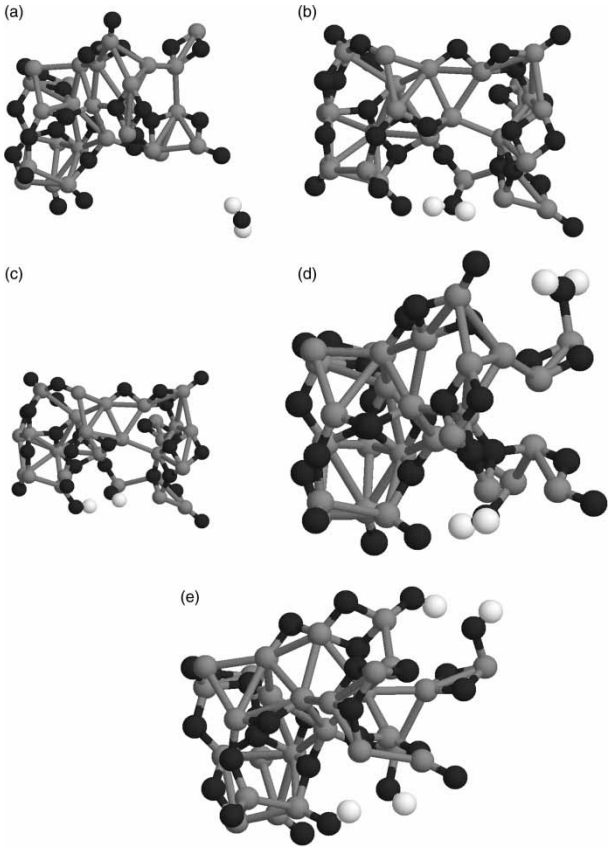

Figure 6. The 27SiOW and 27SiO2W systems, denoting the QC-optimised configurations through the reaction of the 27SiO cluster with the 1 and 2 water molecules, respectively: (a) 27SiOW starting configuration, water molecule, (b) sorbed at the 27SiO cluster surface, (c) dissociation of the water molecule, (d) two water molecules, sorbed at the 27SiO cluster surface and (e) the dissociation of two water molecules at the 27SiO cluster surface.

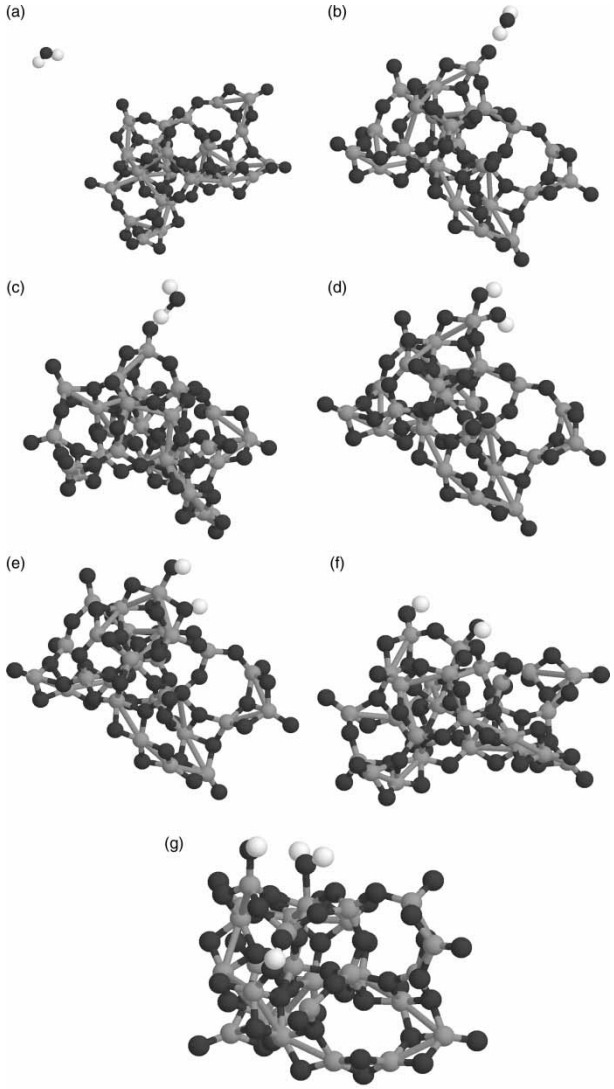

Figure 7. The 27SiO2_W and 27SiO2_2W systems, denoting the QC-optimised configurations along the reaction of the 27SiO2 densified silica cluster with the 1 and 2 water molecules, respectively: (a) 27SiO2_W starting configuration, water molecule, (b) sorbed at the 27SiO2 cluster surface, (c) metastable configuration of the surface Si—OH group with strongly bonded OH residue, (d) silandiolic $Si(OH)_2$ group in the 27SiO2_W system, (e) dissociation of the water molecule at the 27SiO2 cluster surface with the formation of bridging Si—O(H)—Si group, (f) the resulting 27SiO2_W silica cluster, containing two isolated surface silanol groups and (g) the 27SiO2_2W system, denoting two water molecules, sorbed at the $27SiO_2$ cluster surface.

group ($\Delta E = 24.44$ kJ/mol, $\Delta_r H = -193.58$ kJ/mol). Since the silandiolic group is relatively unstable, one OH-group can migrate to the neighbouring surface silicon atom, forming the bridging Si—O(H)—Si group ($\Delta E = 91.64$ kJ/mol, $\Delta_r H = 81.23$ kJ/mol) first, and then forming the monosilanol group ($\Delta E = 55.82$ kJ/mol, $\Delta_r H = -109.91$ kJ/mol). The resulting silica nanoparticle contains two isolated surface silanol groups. The overall enthalpy of the reaction of the $27SiO_2$ nanoparticle with the water molecule is equal to -184.63 kJ/mol.

The hydroxylation of the densified silica nanoparticle is a complex reaction and it can cease at the stage of silandiolic $Si(OH)_2$ group formation. This behaviour of the densified silica (silica fume) contrasts with the behaviour of the fumed silica (aerosil) nanoparticle, where the hydroxylation is a one-stage process, leading to the formation of two H-bonded OH-groups only, with the enthalpy of the reaction equal to -340.75 kJ/mol ($\Delta E = 101.47$ kJ/mol) [37]. This fact causes the differences in the high-frequency region of the IR spectra of the silica fume and the fumed silica.

The second water molecule absorbs on the surface of the hydroxylated densified silica, forming two H-bonds with the hydroxyl groups (Figure 7(g)). This cluster has been used for the QC simulation of the high-frequency region of the silica fume IR spectrum. The part of QC-simulated IR spectrum,

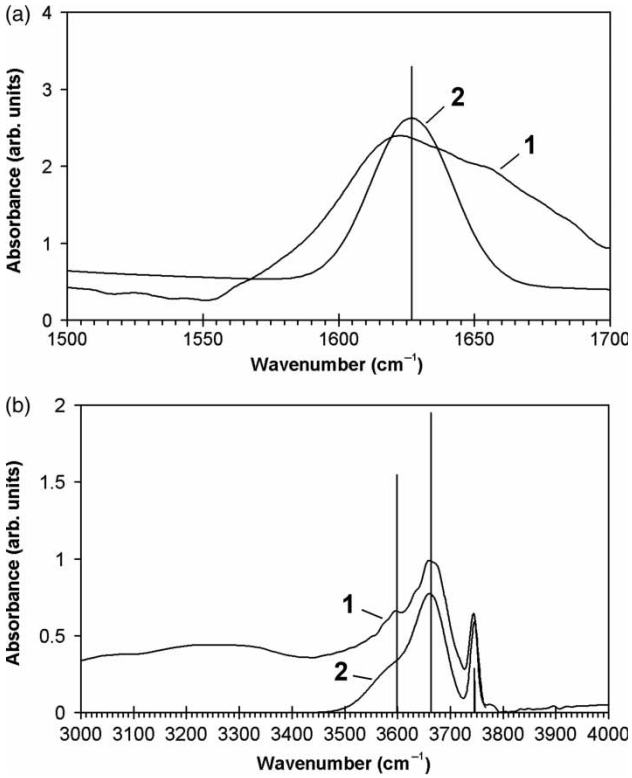

Figure 8. The QC-simulated IR spectrum of the $27SiO_2$ cluster with two sorbed water molecules (27SiO2_2W), fitted to the experimental DRIFT: (a) water molecules deformation vibration $\delta(H_2O)$ region; (b) water and surface hydroxyl groups stretch ν(O—H) vibrations region. Line (1) – experimental spectrum, line (2) – simulated spectrum. Delta functions of the QC-simulated vibrational modes are represented as thin solid sticks in all figures.

fitted to the experimental DRIFT, is shown in Figure 8. Complicated spectrum shape at the region 3000–4000 cm^{-1} reveals the different types of the water and surface hydroxyl group stretch ν(O—H) vibrations. The sharp peak at 3749 cm^{-1} has been assigned to the surface 'free' silanol group stretch ν(O—H) vibrations similar to the fumed silica spectrum. Two overlapping bands at 3598 and 3673 cm^{-1} have been assigned to the symmetrical and anti-symmetrical coordinated water stretch ν(O—H) vibrations, respectively. The coordinated water molecule should have had the deformation vibration $\delta(H_2O)$ at the 1620 cm^{-1}, and this peak has been detected in the experimental spectrum after the mathematical treatment. The mid-low-frequency part of the QC-simulated IR spectrum is similar to the one, discussed earlier (see Section 3.3.2.3).

3.5 Interaction of SiO with CO

3.5.1 Influence of the CO molecules on growth of the SiO cluster

Interaction of SiO molecules with CO in different proportions has been QC examined in order to study the influence of the carbon monoxide on the SiO protoparticle formation. The following seven SiO:CO ratios, identified as clusters 8CO56SiO, 16CO48SiO, 24CO40SiO, 32CO32SiO, 40CO24SiO, 48CO16SiO and 56CO8SiO, have been considered: 56:8, 48:16, 40:24, 32:32, 24:40, 26:48 and 8:56, correspondingly.

The QC simulation has been performed for randomly oriented 64 SiO and CO molecules placed in a cubic lattice 4×4 with the edge equal to 3 nm, used as a starting geometry. The starting models have been obtained by replacing a corresponding quantity of SiO by the CO molecules, similar to what was described in Section 3.4.1. The geometry of the systems has been QC optimised by energy.

The QC-derived data show that the carbon monoxide can react with the SiO and form molecules O═Si—C═O, where the Si—C bond order $W_{Si-C} = 0.3756–0.6328$. This result is in accordance with the literature data on *ab initio* calculations [66], although the cited bond orders are lower. The formation of the carbonyl complex is less energetically preferable than the SiO molecules condensation. Still, the formation of the Si—C coordination bond passivates the SiO molecules and hinders the growth of the SiO protoparticle. At the ratio SiO/CO $\leq$ 1 two or more smaller protoparticles are formed instead of one. The presence of small quantities of the CO in the SiO gaseous mixture does not influence the formation of silicon clusters inside the SiO nanoparticle bulk.

According to the QC-evaluated data, the CO in the final product is bonded to the SiO nanoparticles. The bonded CO may be classified into five structural types, presented at the Figure 9:

(1) simple adsorbed carbon monoxide;
(2) carbon monoxide, coordinated to two neighbouring Si atoms, i.e. bridge carbonyl CO—Si—(C═O)—Si (with Si—Si bond) — ($\mu-2$-group);
(3) carbon monoxide, coordinated to two Si atoms, not bonded directly (silicon atoms may belong to two different particles) – bridge carbonyl CO—Si—(C═O)—Si (without Si—Si bond) – ($\mu-3$-group);
(4) carbon dioxide, formed from carbon monoxide and SiO. (May bound two different protoparticles, too);
(5) bridging carbon monoxide, bonding two particles (unstable form, usually turns into the structural type 4) (Si···C═O···Si — $\mu-1$-group).

Energetic and oxidation stability of the adsorbed CO groups will be discussed in next section.

3.5.2 Interaction of 27SiO nanoparticle with CO. Stability of the adsorbed CO molecules

The QC examination of the interaction of the CO molecule with the 27SiO nanoparticle surface, representing the SiO

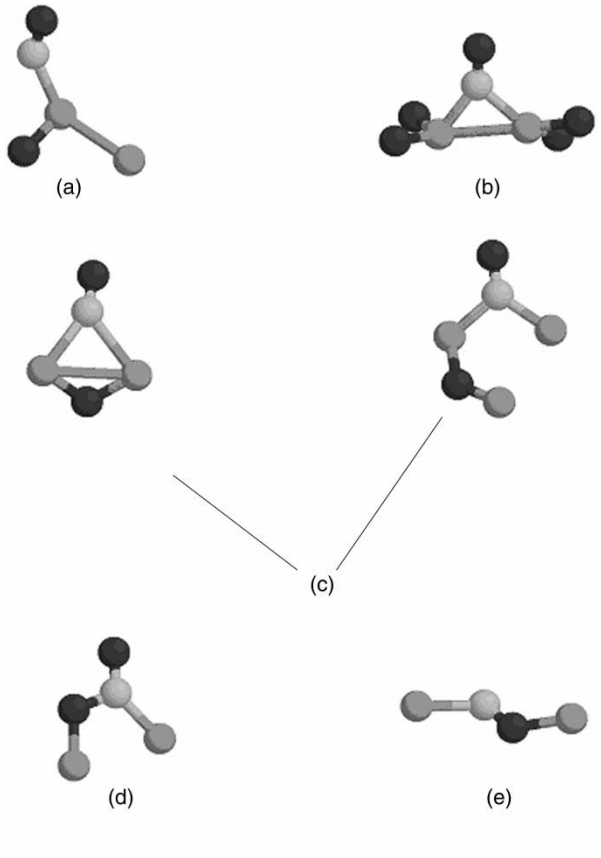

Figure 9. The structural types of the bonded CO: (a) Simple adsorbed carbon monoxide; (b) μ − 2-group; (c) (2 points) μ − 3-group; (d) carbon dioxide, arose from carbon monoxide and SiO; (e) μ − 1-group.

nanoparticle, shows that the sorption occurs with the $\Delta E = 6.13$ kJ/mol, $\Delta_r H = -81.86$ kJ/mol. The spatial structure of the final product is similar to the simple adsorbed carbon monoxide, described in Section 3.5.1.

Though the formation of different types of CO groups on the surface of the SiO nanoparticle is confirmed by the QC calculations, the stability of the products is questionable. The QC examination, based on the 'reaction coordinate' method, proves that the simple adsorbed carbon monoxide (case 1) desorbs as easily as it sorbed on the surface of the SiO, i.e. the reaction is reversible. However, the bridging CO groups (cases 2 and 3, Section 3.5.1) and CO_2 group (case 4, Section 3.5.1) behave as being incorporated into the SiO nanoparticle backbone. At least, the attempts to simulate the desorption reactions failed or led to the reorganisation of the SiO nanoparticle bulk, i.e. the reaction seems to be irreversible. Thus, the CO molecules, incorporated into SiO nanoparticles upon its condensation from SiO molecules, are strongly bonded and might influence the chemical and optical properties of the SiO material.

The QC examination of the oxidation of the SiO nanoparticles with different types of sorbed CO groups, carried out similar to the case of the Section 3.3.2, shows that the oxidation of the SiO bulk ($\Delta_r H \sim -1050$ kJ/mol) is more preferable in regards to energy than the oxidation of the CO to the CO_2 ($\Delta_r H \sim -750$ kJ/mol). The second pathway is also hindered by a relatively high activation barrier ($\Delta E \sim 60$–170 kJ/mol). However, the oxidation of the SiO nanoparticle bulk, together with the formation of SiO_x suboxides, leads to the spontaneous desorption of the CO_2.

4. Conclusions

The silicon clusters inside the SiO bulk, confirmed by QC and Raman studies, are surrounded by the layer of non-stoichiometric SiO_x phase and do not form definitely pronounced domains. The structure of the SiO bulk is completely amorphous and the Si atoms' coordination polyhedra are often different from the tetrahedra.

The mechanism of the SiO high-temperature oxidation is proposed and discussed. It is demonstrated that oxidation occurs through the dissociation of the O_2 molecules. The Si clusters inside the SiO particle are oxidised via the relay-race mechanism, i.e. oxygen-rich SiO_x phase (where $1 < x < 2$) grows continuously upon oxidation. The resulting SiO_2 nanoparticles are densified in comparison with the fumed silica. The QC simulation of the reaction of the densified silica nanoparticle with water shows its reduced reactivity.

Small quantities of the CO in the SiO gaseous mixture do not influence the formation of silicon clusters inside the SiO nanoparticle bulk. At the same time, the CO molecules, incorporated into SiO nanoparticles upon its condensation from SiO molecules, are strongly bonded and might influence the chemical and optical properties of the SiO material.

It is shown that the water molecules form strong H-bond with the SiO superficial atoms but do not dissociate. The influence of CO molecules on the condensation of the SiO molecules and properties of the nanoparticle appears to be of minor importance.

Acknowledgements

We thank Drs J.O. Roszinski and B. Friede for the stimulating discussion and valuable advice.

Notes

1. Email: vkhavr@compchem.kiev.ua
2. Email: lisnyak@univ.kiev.ua
3. This is a metastable configuration.

References

[1] H.-C. Yuan and Z. Ma, *Microwave thin-film transistors using Si nanomembranes on flexible polymer substrate*, Appl. Phys. Lett. 89 (2006), pp. 212105–212107.

[2] M. Tazawa, P. Jin, T. Miki, K. Yoshimura, K. Igrashi, and S. Tanemura, *I.R. properties of SiO deposited on $V_{1-x}W_xO_2$ thermochromic films by vacuum evaporation*, Thin Solid Films 375 (2000), pp. 100–103.

[3] A. Macleod, *Thin Film Optical Filters*, IoP, Bristol, 2001.

[4] P. Jutzi and U. Schubert (eds.), *Silicon Chemistry. From the Atom to Extended Systems*, Wiley-VCH, Weinheim, 2003.

[5] J. Wan, M. Han, J. Zhou, and G. Wang, *Nanofilms of Si clusters confined in SiO nanoparticles prepared by low energy cluster beam deposition*, Phys. Lett. A 280 (2001), pp. 357–360.

[6] S. Veprek and D. Azinovic, *Localization phenomena and photoluminscence from nano-structured silicon, silicon/silicon dioxide nanocomposites, silsesquioxanes and branched polysilanes*, in *Silicon Chemistry. From the Atom to Extended Systems*, P. Jutzi and U. Schubert, eds., Wiley-VCH, Weinheim, 2003, pp. 308–321.

[7] U. Schubert and T. Wieder, *Structure and reactivity of solid SiO*, in *Silicon Chemistry. From the Atom to Extended Systems*, P. Jutzi and U. Schubert, eds., Wiley-VCH, Weinheim, 2003, pp. 242–252.

[8] H. Hofmeister and U. Kahler, *Si Nanocrystallites in SiO_x films by vapour deposition and thermal processing*, in *Silicon Chemistry. From the Atom to Extended Systems*, P. Jutzi and U. Schubert, eds., Wiley-VCH, Weinheim, 2003, pp. 252–269.

[9] G. Hollinger, Y. Jugnet, and T.M. Duc, *Effect of heat treatment on chemical and electronic structure of solid SiO: an electron spectroscopy study*, Solid State Commun. 22 (1977), pp. 277–280.

[10] A. Hohl, T. Wieder, P.A. van Aken, T.E. Weirich, G. Denninger, M. Vidal, S. Oswald, C. Deneke, J. Mayer, and H. Fuess, *An interface clusters mixture model for the structure of amorphous silicon monoxide (SiO)*, J. Non-Cryst. Sol. 320 (2003), pp. 255–280.

[11] B. Friede and M. Jansen, *Some comments on so-called 'silicon monoxide'*, J. Non-Cryst. Sol. 204 (1996), pp. 202–203.

[12] B. Friede, *Neue Beiträge zur Darstellung und Struktur subvalenter Silicium-, Germanium- und Zinnchalkogenide*, Ph.D. diss., Rheinischen Friedrich-Wilhelms University, 1999.

[13] I.P. Lisovskii, V.G. Litovchenko, V.B. Lozinskii, S.I. Frolov, E.G. Schmidt, H. Flietner, and W. Fussel, *I.R. study of short-range and local order in SiO_2 and SiO_x films*, J. Non-Cryst. Sol. 187 (1995), pp. 91–95.

[14] F. Yubero, A. Barranco, J.P. Espinos, and A.R. Gonzalez-Elipe, *Anomalous behaviour in resonant Auger emission of SiO_x thin films*, Surf. Sci. 436 (1999), pp. 202–212.

[15] A. Faessler and H. Krämer, *Über die Existenz der Oxydationsstufen Si_2O, SiO und Si_2O_3 des Siliciums*, Ann. Phys. 459 (1959), pp. 263–268.

[16] M.T. Costa Lima and C. Senemaud, *Electronic distribution of SiO by X-ray spectroscopy*, Chem. Phys. Lett. 40 (1976), pp. 157–159.

[17] J.R. McCreary, R.J. Thorn, and L.C. Wagner, *Valence states in condensed silicon monoxide*, J. Non-Cryst. Sol. 23 (1977), pp. 293–297.

[18] H. Schnöckel and R. Köppe, *Reactions with matrix isolated SiO molecules*, in *Silicon Chemistry. From the Atom to Extended Systems*, P. Jutzi and U. Schubert, eds., Wiley-VCH, Weinheim, 2003, p. 20; T. Mehner, H.J. Gocke, S. Schunck, und H. Schnöckel, *Dimeres SiO_2 Matrix-I R-Untersuchungen und* ab initio *SCF-Rechnungen*, Z. Anorg. Allg. Chem. 580 (1990), p. 121; T. Mehner, R. Köppe, and H. Schnöckel, *IR-spektroskopischer Nachweis von [PdSiO]*, Angew. Chem. Int. Ed. 31 (1992), p. 638; A. Weiss and A. Weiss, *Über Siliciumchalkogenide. VI. Zur Kenntnis der faserigen Siliciumdioxyd-Modifikation*, Z. Anorg. Allg. Chem. 276 (1954), p. 95.

[19] M. Friesen, M. Junker, A. Zumbusch, and H. Schnöckel, *Raman-spectroscopy of oligomeric SiO species isolated in solid methane*, J. Chem. Phys. 111 (1999), pp. 7881–7887.

[20] O.V. Khavryuchenko, V.D. Khavryuchenko, J.O. Roszinski, A.I. Brusilovets, B. Friede, and V.V. Lisnyak, *Spectral and quantum chemical examination of the Si clusters nascent inside the SiO bulk*, Thin Solid Films 515 (2006), pp. 1280–1285.

[21] G. Pérez, A.M. Bernal-Oliva, E. Márquez, J.M. González-Leal, C. Morant, I. Génova, J.F. Trigo, and J.M. Sanz, *Optical and structural characterisation of single and multilayer germanium/silicon monoxide systems*, Thin Solid Films 485 (2005), pp. 274–283.

[22] K. Schulmeister and W. Mader, *TEM investigation on the structure of amorphous silicon monoxide*, J. Non-Cryst. Sol. 320 (2003), pp. 143–150.

[23] J. Wang, X.F. Wang, Q. Li, A. Hryciw, and A. Meldrum, *The microstructure of SiO thin films: from nanoclusters to nanocrystals*, Philos. Mag. 87 (2007), pp. 11–27.

[24] T. Iwase, K. Azuma, M. Watanabe, T. Ogasawara, and Y. Natsume, *Sintered object of silicon monoxide and method for producing the same*, US Patent No 7,151,068, 2006.

[25] A. Schei, J.Kr. Tuset, and H. Tveit, *Production of high silicon alloys*, Tapir Acad. Publ., Trondheim, 1998.

[26] ACI 234R-96 American Concrete Institute report, *Guide for the Use of Silica Fume in Concrete*, T.C. Holland, ed., ACI Committee 234, 1996, pp. 234R1–234R51.

[27] W. Poch and A. Dietzel, *The formation of silicon carbide from silicon dioxide and carbon*, Ber. Dtsch. Keram. Ges. 39 (1962), pp. 413–426.

[28] S. Gjerstad, *Chemical metallurgical investigation concerning carbothermic reduction of alumina and silica*, Ph.D. diss., Norwegian University of Science and Technology, 1968.

[29] K. Wiik, *Kinetics and reaction between silica and carbon*, Ph.D. diss., Norwegian University of Science and Technology, 1990.

[30] G. Gudmundsson and H. Olafsson, *Alkali-silica reactions and silica fume 20 years of experience in Iceland*, Cem. Concr. Res. 29 (1999), pp. 1289–1297.

[31] I. Natkaniec, S.I. Bragin, J. Brankowski, and J. Mayer, *Multicrystal inverted geometry spectrometer NERA-PR at the IBR-2 pulsed reactor*, in *Proc. ICANS XII*, Abingdon, RAL Report No. 94–025, vol. I, 1993, pp. 89–96.

[32] E. Sheka, V. Khavryutchenko, and I. Markichev, *Technological polymorphism of disperse amorphous silicas: inelastic neutron scattering and computer modelling*, Russ. Chem. Rev. 64 (1995), pp. 389–415.

[33] E.F. Sheka and V. Khavryutchenko, *Nanomaterials: reality and computational modelling*, NanoStruct. Mater. 6 (1995), pp. 803–806.

[34] V.D. Khavryuchenko, O.V. Khavryuchenko, and V.V. Lisnyak, *Quantum chemical insight on vibration spectra of silica systems*, Mol. Sim. 33 (2007), pp. 531–540.

[35] D.C. Young, *Computational Chemistry: A Practical Guide for Applying Techniques to Real-World Problems*, Wiley, New York, 2001.

[36] H.B. Schlegel, *Optimization of equilibrium geometries and transition structures*, Adv. Chem. Phys. 67 (1987), pp. 249–286.

[37] V.D. Khavryutchenko, H. Barthel, and E. Nikitina, *Fumed silica synthesis: from molecules, protoparticles and primary particles to aggregates and agglomerates*, Macromol. Symp. 169 (2001), pp. 7–18.

[38] E. Nikitina, V. Khavryutchenko, E. Sheka, H. Barthel, and J. Weis, *Intermolecular interactions of polydimethylsiloxane oligomers with hydroxylated and silylated fumed silica. Quantum-chemical modeling*, Compos. Interfaces 6 (1999), pp. 3–17.

[39] J.J.P. Stewart, *Optimization of parameters for semiempirical methods II. Applications*, J. Comp. Chem. 10 (1989), pp. 221–264.

[40] J.J.P. Stewart, *PM3*, Encycl. Comput. Chem. 3 (1998), pp. 2080–2086.

[41] W. Weber and W. Thiel, *Orthogonalization corrections for semiempirical methods*, Theor. Chem. Acc. 103 (2000), pp. 495–506.

[42] P. Khan, K.K. Das, and S.P. Bhattacharyya, *On the connection between semiempirical molecular orbital theories and effective hamiltonians: A constrained variational point of view*, Int. J. Quant. Chem. 37 (1990), pp. 415–422.

[43] A.V. Khavryutchenko and V.D. Khavryutchenko, *Quantum chemistry simulation of 60-fullerene: interaction under external pressure*, Z. Naturforsch. A 60 (2005), pp. 41–46.

[44] V. Khavryutchenko, J. Garapon, and B. Poumellec, *Structure simulation of silica glasses: approach to CVD*, Model. Simul. Mater. Sci. Eng. 9 (2001), pp. 465–483.

[45] E.F. Sheka, V.D. Khavryutchenko, and E.A. Nikitina, *From molecules to particles: quantum-chemical view applied to fumed silica*, J. Nanopart. Res. 1 (1999), pp. 71–81.

[46] V. Khavryutchenko, E. Sheka, D.H. Huang, and M. Aono, *Supercluster quantum-chemical approach to the Si(111)7 × 7 surface. 2. Charge and spin distribution*, Phys. Low-Dim. Struct. 3–4 (1998), pp. 81–106.

[47] V. Khavryutchenko, E. Sheka, D.H. Huang, and M. Aono, *STM individual atom manipulation on Si(111)7 × 7surface: computational modeling*, Phys. Low-Dim. Struct. 9–10 (1996), pp. 15–43.
[48] V.D. Khavryuchenko, O.V. Khavryuchenko, and V.V. Lisnyak, *Quantum chemical simulation of relaxation and thermally stimulated processes: A vibration excitation-relaxation stochastic optimization*, Z. Naturforsch. A 60 (2005), pp. 797–804.
[49] W.S. Verwoerd and K. Weimer, *Comparison of semiempirical calculations for silicon compounds*, J. Comput. Chem. 12 (1991), pp. 417–420.
[50] V. Khavryutchenko, *Computation vibration spectroscopy as a tool for investigation of complicated systems*, Euras. Chem. Tech. J. 6 (2004), pp. 157–170.
[51] K. Hołderna-Natkaniec, A. Szyczewski, I. Natkaniec, V.D. Khavryutchenko, and A. Pawlukojc, *Progesterone and testosterone studies by neutron-scattering methods and quantum chemistry calculations*, Appl. Phys. A 74 (2002), pp. S1274–S1276.
[52] E. Sheka, I. Natkaniec, V. Khavryutchenko, E. Nikitina, H. Barthel, and J. Weis, *INS study of intermolecular interaction at the silicone-fumed silica interface*, Phys. B 276–278 (2000), pp. 244–246.
[53] K. Hołderna-Natkaniec, I. Natkaniec, J. Kalus, and V.D. Khavryutchenko, *Neutron spectrometry and numerical simulations of low-frequency internal vibrations in solid xylenes*, AIP Conf. Proc. 479 (1999), pp. 191–194.
[54] K. Hołderna-Natkaniec, I. Natkaniec, and V.D. Khavryutchenko, *Low frequency internal vibrations of norbornane and its derivatives studies by INS and Quantum chemical calculations*, AIP Conf. Proc. 479 (1999), pp. 187–190.
[55] K.A. Wiberg, *Application of the pople-santry-segal CNDO method to the cyclopropylcarbinyl and cyclobutyl cation and to bicyclobutane*, Tetrahedron 24 (1968), pp. 1083–1096.
[56] I. Mayer, *Charge, bond order and valence in the AB initio SCF theory*, Chem. Phys. Lett. 97 (1983), pp. 270–274.
[57] I. Mayer, *Bond order and valence indices a personal account*, J. Comput. Chem. 28 (2007), pp. 204–221.
[58] R. Ponec, *Chemical bonding in solids. On the generalization of the concept of bond order and valence for infinite periodical structures*, Theor. Chem. Acc. 114 (2005), pp. 208–212.
[59] A.B. Sannigrahi, Ab initio *molecular orbital calculations of bond index and valency*, Adv. Quant. Chem. 23 (1992), pp. 301–351.
[60] H. Schnöckel, T. Mehner, H.S. Plitt, and S. Schnuck, *Structure of $(SiO)_2$, a comparison between $(AlF)_2$, $(SiO)_2$, and $(PN)_2$ matrix infrared investigation* ab initio *calculation*, J. Am. Chem. Soc. 111 (1989), pp. 4578–4582.
[61] A. Hohl, T. Weider, V. Joco, and H. Fuess, *Radial distribution function of silicon monoxide (SiO)*, ILL Reports, Grenoble, 1999, http://www.ill.fr/.
[62] S. Hasegawa, L. He, T. Inokuma, and Y. Kurata, *Vibrational properties of SiO and SiH in amorphous SiO_x:H films ($0 \leq x \leq 2.0$) prepared by plasma-enhanced chemical vapor deposition*, J. Non-Cryst. Sol. 185 (1995), pp. 249–261.
[63] A. Lee Smith, *Applied Infrared Spectroscopy: Fundamentals, Techniques and Analytical Problem-Solving*, Wiley-Interscience, New York, 2001.
[64] W.C. Price and K.S. Tetlow, *Infrared christiansen. Filter effect in slurries of organic crystals*, J. Chem. Phys. 16 (1948), pp. 1157–1162.
[65] R. Burgert, H. Schnöckel, A. Grubisic, X. Li, S.T. Stokes, K.H. Bowen, G.F. Ganteför, B. Kiran, and P. Jena, *Spin-conservation accounts for aluminium cluster reactivity pattern with O_2*, Science 319 (2008), pp. 438–442.
[66] L. Zhang and Q.-Z. Qin, *A theoretical study on the novel molecule OSiCO and its isomers*, Chem. Phys. Lett. 326 (2000), pp. 494–500.

Supporting Information Available: The starting and final structures of the simulated clusters as well as the animations of the optimisation pathways are available online at http://www.informaworld/gmos.